An analytic model of the incompressible one-phase clearance flow in liquid injected screw expanders

M. Gräßer, **A. Brümmer**, TU Dortmund University, Dortmund

Abstract

Operation performance of screw expanders is significantly influenced by different clearance types. Clearances are necessary to ensure safety and reliability, but resulting dissipative internal leakage flows usually reduce quality of energy conversion. Therefore, understanding flow processes within different clearances is essential. Assuming that an injected auxiliary liquid seals the clearances, an analytic model of incompressible one-phase flow is developed in order to calculate incompressible clearance mass flow and power resulting from frictional effects on the rotor´s surface. In contrast to numerical approaches, major advantages of an analytical model are short computing times and clear physical dependencies which enable a better understanding of flow processes.

Moving boundary and pressure difference between clearance in- and outlet are driving forces of clearance flows in screw machines. Therefore, the flow model is based on superposed Couette-Poiseuille flow which is described for laminar and turbulent flow processes. In addition, an initial evaluation of several assumptions is received by comparing analytical results of parallel walls with computational fluid dynamics (CFD) simulation. Initially, front clearances and housing clearances are analysed. An abstraction of their geometries is given and the results are discussed in detail.

Introduction

At present operational performance of one–phase rotary displacement machines is mainly calculated using chamber model based simulations [1, 2]. In order to achieve a satisfying agreement between simulation and measurement, an accurate model of internal clearance flows is indispensable. Compressible one-phase clearance flows in screw machines have been studied intensively. *Fister and Neumann* [3] estimate flow and heat coefficients as well as dissipation loss within different clearance types by applying a finite difference method to simplified geometries. A semi-empirical approach to determine the influence of different clearances on indicated and volumetric efficiency is presented by *Fleming and Tang* [4]. In 2002 *Sachs* [5] succeeded in visualizing gas flow through a static male rotor housing clearance of a compressor by means of Toepler´s “schlieren method”. Negligible influence of

the rotor´s circumferential speed is demonstrated and initial numeric simulations with the commercial software package FLUENT are presented. In addition *Kauder and Stratmann* [6] point out the effect of different turbulence models.

Operation performance of screw machines is significantly influenced by appearance of liquid fluid phase within the working chamber, for example by injecting auxiliary liquid or by condensation of working fluid. Yet, presently it is not possible to simulate two-phase rotary displacement machines in reasonable accordance to experimental results. The impact of oil injection into a screw compressor is qualitatively described by *Kauder´s* "Oil-Surge-Theory" [7]. According to this approach, clearances will be closed completely by auxiliary liquid which leads to smaller clearance flows of working fluid, but also to higher friction losses. An initial model of oil distribution within screw compressors is given by *Harling* [8] who uses various analytic models of incompressible, laminar flow through different clearance types. Similarly *Wincek* [9] models circumferential clearance flow of a screw pump by superposed, laminar, incompressible Couette-Poiseuille flow.

Nevertheless, a sufficient qualitative and quantitative model of two-phase clearance flows in screw machines does not exist. In contrast to compressible flow, drag force of the rotor will not be negligible for incompressible auxiliary liquid flow. Furthermore turbulences might occur which have not been modeled for incompressible clearance flows of screw machines. The superior research objective is the simulation of two-phase screw machines which requires proper understanding of clearance flows at moderate computing times. Therefore this paper presents an initial analytic model of incompressible one-phase clearance flow which can be applied to front and housing clearances of screw machines. In addition, some modelling assumptions will be compared to numeric simulations with the commercial software ANSYS CFX.

Modelling of laminar and turbulent flow through parallel moving walls

Initially a model of static, incompressible flow through parallel moving walls is developed. Subsequently the complex geometry of front and housing clearances will be described by a finite number of wall elements which are connected serially or in parallel. Assuming laminar, two dimensional flow, negligible transverse velocity ($c_y \ll c_x$) and constant pressure gradient dp/dx as well constant wall velocity C at one side, flow velocity

$$c_x(y) = \frac{dp}{dx}\frac{1}{\eta}\left(\frac{1}{2}y^2 - \frac{h}{2}y\right)\Big|_{\text{Poiseuille flow}} - \frac{C}{h}y\Big|_{\text{Couette flow}}. \qquad (1)$$

is derived by the differential conservation equations of mass and momentum. **Figure 1** shows the relative Cartesian coordinate system fixed on the static wall. Furthermore, qualitative velocity profiles of superposed Couette-Poiseuille flow are given for positive and negative algebraic sign of wall velocity C. The first summand of equation (1) corresponds to Poiseuille flow whereas the second part represents Couette flow [10]. Hence there are no interactions between these partial flows as the exact solution of the differential equations is superposed Couette-Poiseuille flow. Following mass flow and wall shear stress are also an additive combination of the partial solutions. By comparing Reynolds numbers of laminar flow with critical Reynolds numbers given by *Schlichting* [10]

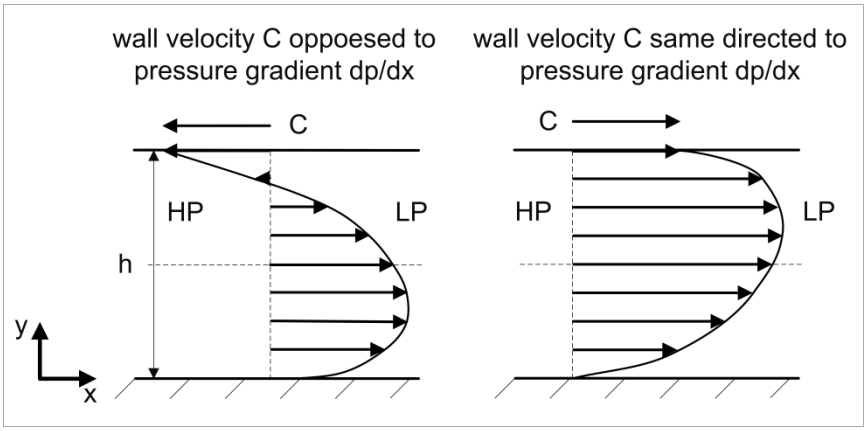

Fig. 1: Qualitative flow profiles of laminar Couette-Poiseuille flow between parallel moving walls
(HP / LP: high/ low pressure side)

$$Re_{crit,C} = 1300 \quad \text{and} \quad Re_{crit,P} = 3000. \tag{2}$$

the assumption of a laminar flow is surveyed. These Reynolds numbers depend on fluid properties, mean velocity and characteristic length of slender channels which is 2h. Flow type strongly depends on which auxiliary liquid is used. Clearance flow of water is turbulent for most interesting operating points whereas typical compressor oil flows are laminar. In order to develop a model which is valid for various auxiliary liquids, the laminar flow model between parallel walls will be extended by a turbulent flow model derived separately for Couette and Poiseuille flow. **Figure 2** illustrates the qualitative velocity profile of turbulent Couette flow. By reasons of symmetry, the areas A_1 and A_2 must have the same size. Thus Couette mass flow is independent of either laminar or turbulent flow type and can be calculated by

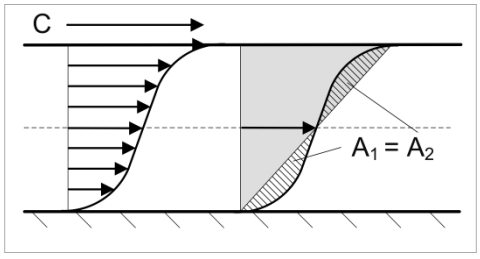

Fig. 2: Qualitative turbulent Couette flow profile [10]

$$\dot{m}_C = \rho w h c_m = \rho w \int_0^h c(y)dy = \frac{\rho w h C}{2}. \tag{3}$$

Wall shear stress of turbulent Couette flow is derived from incompressible, static, two-dimensional, time-averaged Navier-Stokes equations originally introduced by Reynolds [10]. Relation between mean velocity and time-averaged wall shear stress is given by the law of resistance of Couette flow. Therefore wall shear stress is calculated by inverting this relation to

$$\tau_{w,C} = C^2 \frac{\rho}{4} \left(\kappa \ln^{-1} \left(\frac{C^2 h}{2\nu} \right) G(K,D) \right)^2 \tag{4}$$

where K and D are mathematical constants of C,h,v, roughness of the wall and turbulent modelling. The values of function G(K,D) are tabulated by *Gersten and Herwig* [11]. In this paper turbulence model of eddy viscosity is used to close the set of equations. The eddy viscosity function of Couette flow is given by *Schlichting* [10]. Note that mass flow as well as transferred wall shear stress of turbulent Couette flow are calculated without knowing the exact velocity profile. There are velocity functions for both boundary and core layer; however, there is no analytic transition function and the exact location of transition is unknown.

Assuming a completely developed velocity profile, wall shear stress of Poiseuille flow is independent of flow type. From the integral conservation of momentum follows

$$\tau_{w,P} = -\frac{dp}{dx}\frac{h}{2}. \tag{5}$$

for laminar and turbulent flow. Notably, wall shear stress neither depends on laminar or turbulent flow type nor on the fluid. Mass flow will be derived from time-averaged mean velocity

$$c_{m,P} = \sqrt{\frac{\tau_{w,P}}{\rho}} \left(\frac{1}{\kappa} \ln \left(\frac{h\rho}{2\eta} \sqrt{\frac{\tau_{w,P}}{\rho}} \right) + 3.4 \right), \tag{6}$$

which is related to wall shear stress by the law of resistance of Poiseuille flow. The constant value 3.4 is valid for hydraulic smooth walls and eddy viscosity turbulent modelling described in [10]. Again, mass flow and wall shear stress can be calculated for turbulent flow although the complete velocity profile is unknown.

Currently no analytic model for turbulent Couette-Poiseuille flow exists. Due to this deficiency, combined flow will be modelled by superposition which implies negligence of

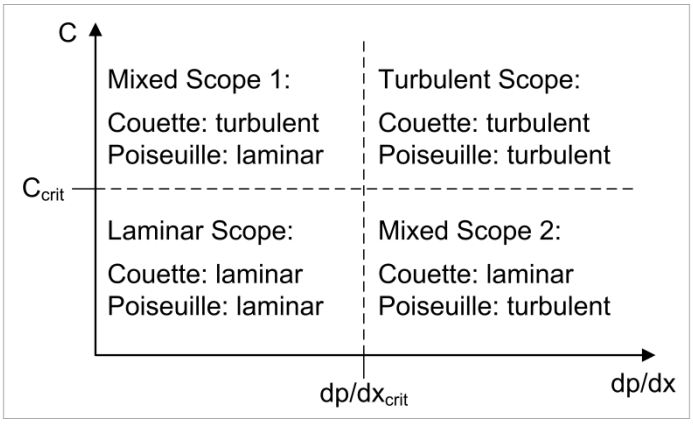

Fig. 3: Scopes of modelling

interdependencies between Couette and Poiseuille flow. Furthermore a sudden transition of laminar and turbulent flow is assumed. The point of transition, which depends on operational parameters and flow geometry, is given by the critical Reynolds numbers in equation (2). A critical Reynolds number for combined flow was not found in literature. **Figure 3** shows different scopes of modelling that result. Although flows of mixed scopes are obviously turbulent one partial flow is calculated laminar as the turbulent model cannot be used for low partial Reynolds number. Nevertheless, uncertainties of the model might not be too serious as laminar flow is usually negligible compared to turbulent flow for mixed scopes. Thus a model to calculate laminar and turbulent Couette-Poiseuille flow between plane walls was developed. Subsequently, analytic results will be compared to numeric simulations.

Comparison of analytic flow between parallel walls with computational fluid dynamics

In order to evaluate the model described above, results for water (ϑ = 25°C = const.) will be compared to numeric simulation using the commercial software ANSYS CFX. Calculations are made with structured mesh of 1201x149x2 cells, in order to simulate two-dimensional flow. Cell distribution along the direction of flow (x) and the core layer (y) is linear, whereas boundary layer (y) has exponential cell distribution. Static pressure at in- and outlet as well as wall velocities are given boundary conditions. The κ-ω-Modell is used to describe turbulence effects.

Figure 4 illustrates velocity profiles of turbulent Couette flow simulated analytical and numerical. Additionally mass flow and wall shear stress are given. As mass flow depends linearly on clearance width, values are given per meter. Analytic velocity profile of Couette flow matches well with the numeric solution. As previously mentioned, there is no analytic transition function between boundary and core layer. In the near-wall region numeric velocity profile is almost identical with analytic boundary layer function, whereas in the middle of clearance ($0.025 < y < 0.075$) it corresponds to analytic core layer. Furthermore the resulting mass flows are identical; however, transferred wall shear stresses differ by about 12%, which is an acceptable high degree of variation.

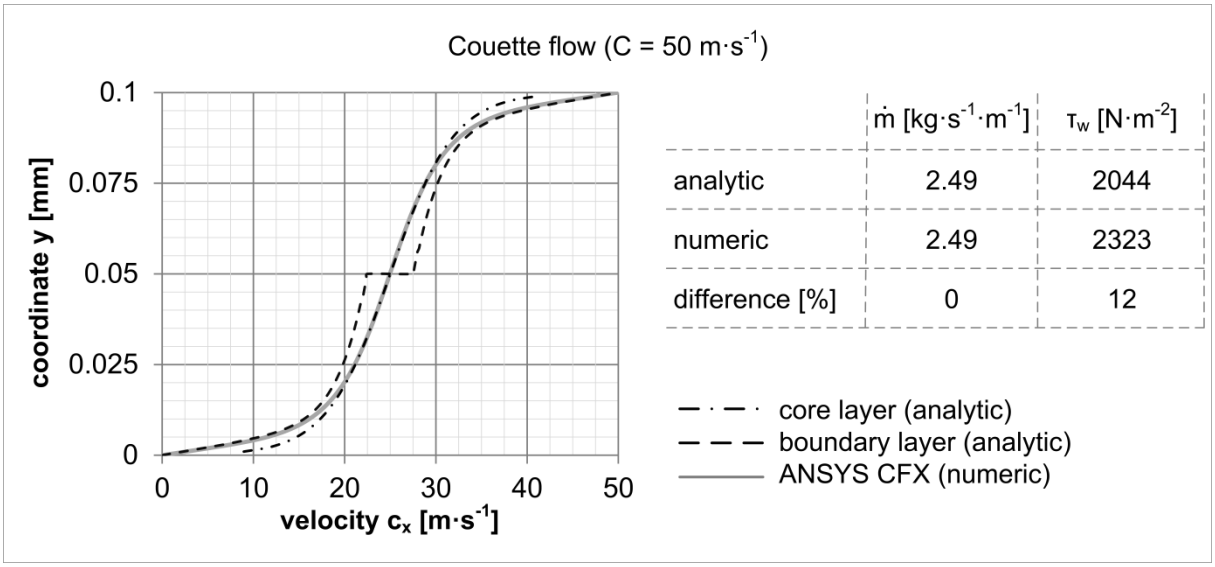

	$\dot{m}$ [kg·s^{-1}·m^{-1}]	τ_w [N·m^{-2}]
analytic	2.49	2044
numeric	2.49	2323
difference [%]	0	12

Fig. 4: Analytic and numeric velocity profile of turbulent Couette flow at high Reynolds numbers (Re_{an} = Re_{num} = 5589)

In contrast to turbulent Couette flow, no analytic core layer function for turbulent Poiseuille flow is established. Thus velocity of boundary layer, calculated medium velocity based on equation (6), and analytic maximum velocity of Poiseuille flow are shown in **figure 5**. Analogous to Couette flow, analytic boundary layer function and numeric velocity profile match very well in the near-wall region. Nevertheless, analytical simulations yield to mass flow which is 12% greater than numerically calculated mass flow. This difference results from the high medium velocity calculated from equation (6) shown in figure 5. Consequently

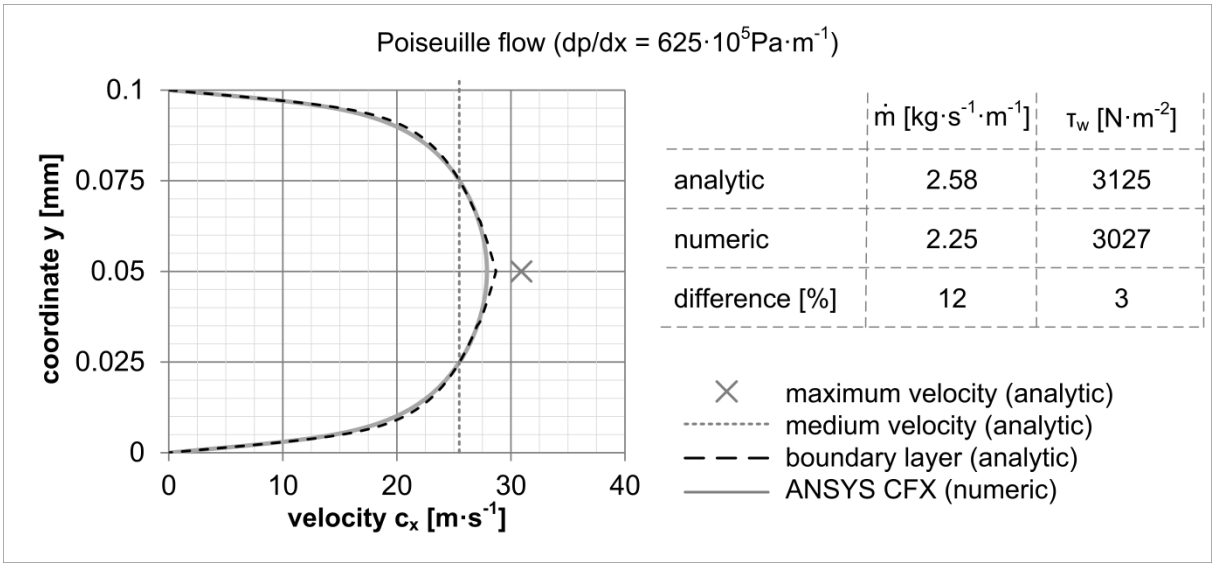

	$\dot{m}$ [kg·s^{-1}·m^{-1}]	τ_w [N·m^{-2}]
analytic	2.58	3125
numeric	2.25	3027
difference [%]	12	3

Fig. 5: Analytic and numeric velocity profile of turbulent Poiseuille flow at high Reynolds numbers (Re_{an} = 5791; Re_{num} = 5050)

Reynolds numbers vary according to the simulation used. Also maximum velocity of the analytic model is greater than maximum velocity of the numeric solution. In contrast, deviation of transferred wall shear stresses accounts for only 3%.

Proceeding, the assumed superposition, that is linearly combined Couette and Poiseuille flow, will now be evaluated for variation of wall velocity and dp/dx constant at $625 \cdot 10^5 Pa \cdot m^{-1}$. There is no reasonable superposed velocity profile from analytic simulations as analytic velocity curves of single flows shown in figure 4 and 5 are incomplete. Thus mass flow per meter and transferred wall shear stress of superposed simulations are compared to directly combined numeric simulation of Couette-Poiseuille flow, **figure 6**. Due to deviation between numeric and analytic values of single Couette and Poiseuille flow (figure 4 and 5) superposition is shown for both analytic and numeric single simulation. This difference is Δ_1 whereas influence of superposition is described by Δ_2.

It is obvious that constant difference of superposed analytic and numeric mass flow $\Delta_{1,\dot{m}}$ is based on deviation of single Poiseuille flow (figure 5). Numeric mass flow of combined simulation is even smaller than numeric superposed mass flow which is most probably based on the nonlinear turbulent viscosity. Thus difference $\Delta_{2,\dot{m}}$ increases with the wall velocity. Deviations of wall shear stress are explained analogous. Difference $\Delta_{1,\tau}$ mainly results from various wall shear stresses of pure Couette flow (figure 4). Again higher turbulent viscosity of combined flow leads to higher transferred shear stress on the rotor. Nevertheless, difference $\Delta_{2,\tau}$ seems to be almost independent of the wall velocity. Overall the shown differences are acceptable.

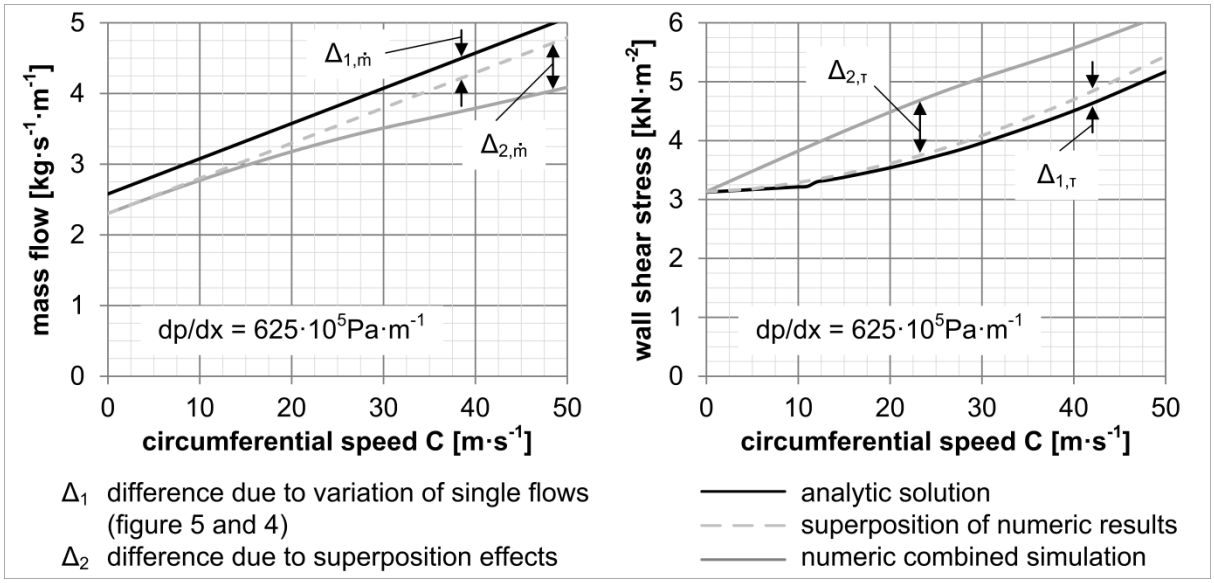

Fig. 6: Comparison of numerically simulated mass flow and shear stress of Couette-Poiseuille flow with superposed results

Definitions and boundary conditions for transferring parallel wall model to clearances of screw type machines

In order to simulate incompressible one-phase clearance flow of screw compressors and screw expanders the system of parallel walls is applied to the complex geometry of front and housing clearances. **Figure 7** shows the rotor pair of the GL51 screw type machine investigated exemplarily herein. The modified asymmetric SRM profile has a root and crown circle diameter of d_{rc} = 34.86 mm and d_{cc} = 71.84 mm respectively. Cartesian coordinate systems of front and housing clearance are demonstrated. In order to calculate clearance mass flow between consecutive chambers, both coordinate systems are fixed on the rotor. Thus the housing moves with relative circumferential speed, whose direction depends on the application of screw machine as expander and compressor respectively. Chamber numbering is absolute and does not change with screw type application. Pressure difference at both clearances is defined as

$$\Delta p_{clearance} = p_2 - p_1. \tag{7}$$

Therefore during the working cycle of a screw machine, negative pressure differences are dominant as pressure in chamber 1 is usually higher than pressure in chamber 2. Nevertheless, overexpansion or overcompression result in reversed pressure differences at both clearances. Mass flow from chamber 1 to chamber 2 is defined as positive while opposite direction is indicated by a negative algebraic sign. Power transferred from fluid to rotor due to friction is calculated by multiplying integrated shear stress along the clearance by circumferential speed. A positive algebraic sign of power indicates the fluid´s power consumption whereas negative power corresponds to power that drives the rotor.

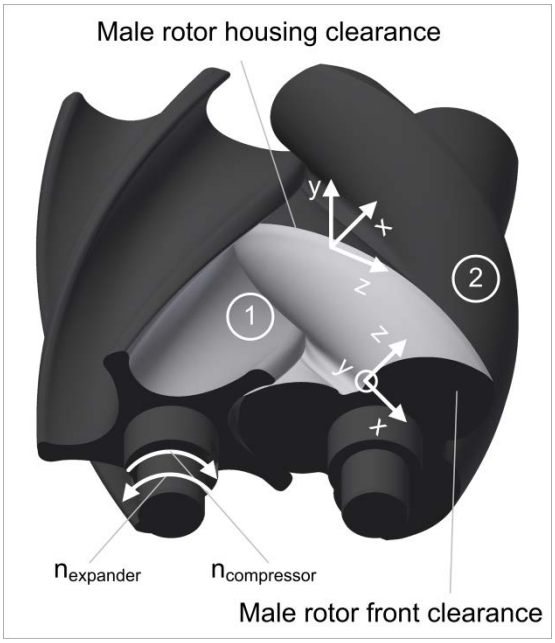

Fig. 7: Coordinate systems and chamber definition at front and housing clearance of the GL51 screw type machine

Modelling of flow through front clearances

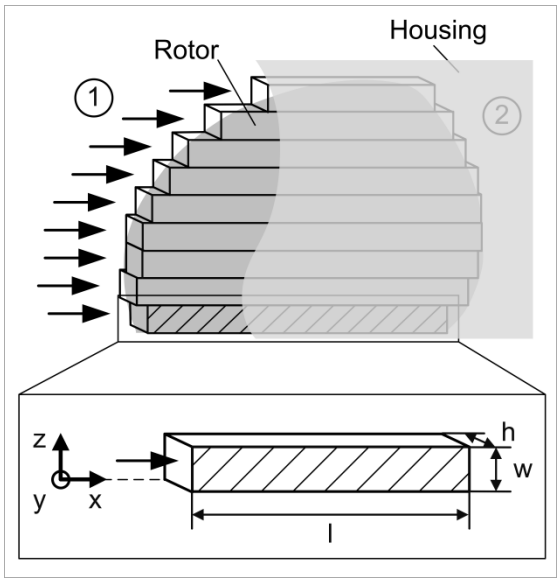

Fig. 8: Modelling front clearance by finite number of wall elements

In this chapter the model of laminar and turbulent Couette-Poiseuille flow between parallel walls will be applied to front clearances. **Figure 8** shows front clearance geometry modelled by a finite number of wall elements connected in parallel. Fluid transport from one element to another is not permitted which implies a negligence of centrifugal forces. Clearance mass flow is given by the sum of mass flow through each element. Subsequently results of a simulation will be shown for compressor as well as for expander.

Simulation results for male rotor front clearance

Illustrated results of incompressible one-phase clearance flow at a male rotor front clearance are calculated for water as auxiliary liquid (ϑ = 25°C = const.). Clearance height is set constant at 0.08 mm. **Figure 9** shows clearance mass flow as a function of pressure

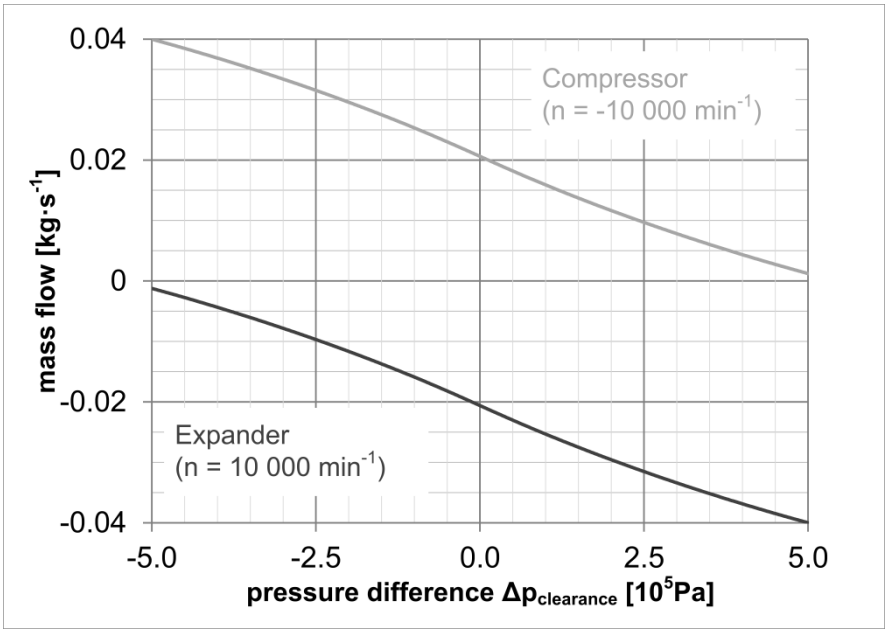

Fig. 9: Mass flow as a function of pressure difference $\Delta p_{clearance}$ for male rotor front clearance of the GL51 screw type machine

difference. Influences of the two operational parameters, rotational speed and pressure difference, are independent of each other. For example, variation in rotational speed leads to a change in Couette flow whereas Poiseuille flow is not affected. It should be recalled that rotational speed for compressors is negatively defined, which leads to linearly increasing Couette mass flow from chamber 1 to chamber 2. Therefore positive mass flow exists due to Couette flow even for vanishing pressure difference. According to equation (7) high pressure in chamber 1 leads to negative defined pressure differences, and the resulting mass flow rises due to additional Poiseuille mass flow. In case of positive pressure differences, Couette and Poiseuille flow counter each other at the compressor´s front clearance. Thus for very high pressure differences, the negative mass flow, which is defined as mass flow from chamber 2 to chamber 1, might result in Couette flow being dominated by Poiseuille flow. In case of an expander, the direction of rotation reverses. Thus the rotor´s drag force causes Couette mass flow from chamber 2 to chamber 1 and the mass flow curve shifts downwards compared to the compressor. Effects of varying pressure difference in an expander are analogous to the compressor application.

Transferred frictional power is illustrated in **figure 10** for both compressor and expander. Apparently pure Couette flow which occurs at a pressure difference of zero leads to dissipative power consumption in both applications due to friction caused by the auxiliary liquid. In case of either negative pressure differences at the compressor´s front clearance or positive pressure differences at the expander´s front clearance braking power increases

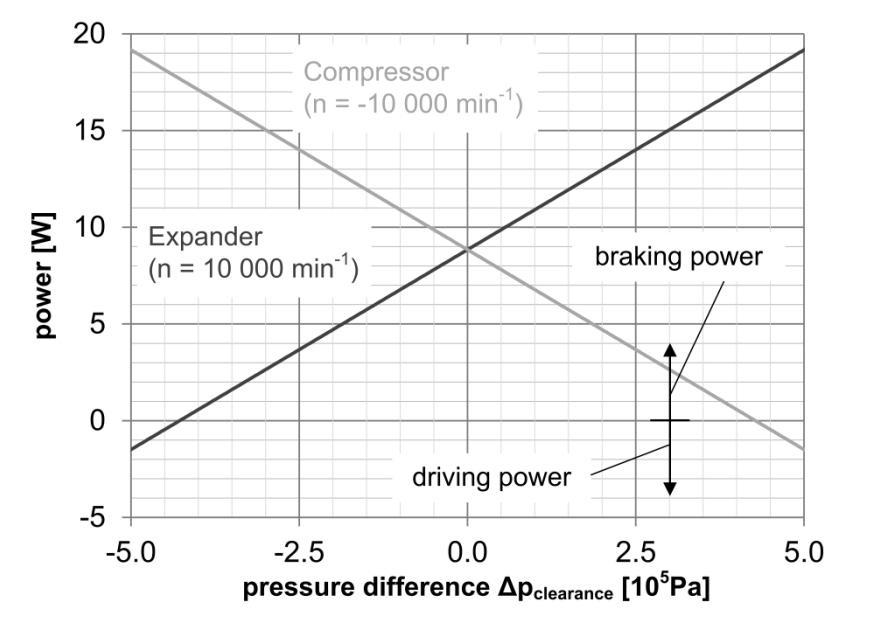

Fig. 10: Transferred frictional power as a function of pressure difference $\Delta p_{clearance}$ for male rotor front clearance of the GL51 screw type machine

based on rising Poiseuille flow which is opposed to the rotor´s moving direction. At the result higher velocity gradients occur on the rotor which leads to increased power consumption due to friction of the flowing fluid. In case of reversed pressure differences in both applications, direction of Poiseuille flow reverses. Thus the overall velocity gradient on the rotor depends on the proportion of the opposed two flows (see also figure 1). It is remarkable that, if the algebraic sign of the velocity gradient changes, the auxiliary liquid even transfers additional power to the rotor. Nevertheless high pressure gradients in the rotor´s direction of motion are required to neutralize negative effects of Couette flow. Appling screw machines as compressor, these high positive pressure differences, which merely exist in case of overcompression, seem to be unlikely. In contrast front clearances of screw expanders might have very high pressure differences at the beginning of working cycle. Notably, vanishing transferred power is not combined with vanishing mass flow. If the overall mass flow equals zero, Couette and Poiseuille flow are opposed and velocity profile consists of flow and backflow that cancel each other out. Nevertheless wall shear stress which causes power transfer exists. It is also possible that combined Couette-Poiseuille flow shows a disappearing velocity gradient directly on the rotor, thus leading to vanishing power. However, in this case non-zero mass flow exists.

An interesting relation between transferred power and operational parameters is demonstrated in **figure 11**. Power is shown as a function of rotational speed for pressure difference constant at $\Delta p_{clearance} = -3 \cdot 10^5$ Pa. At a rotational speed of zero, no power is

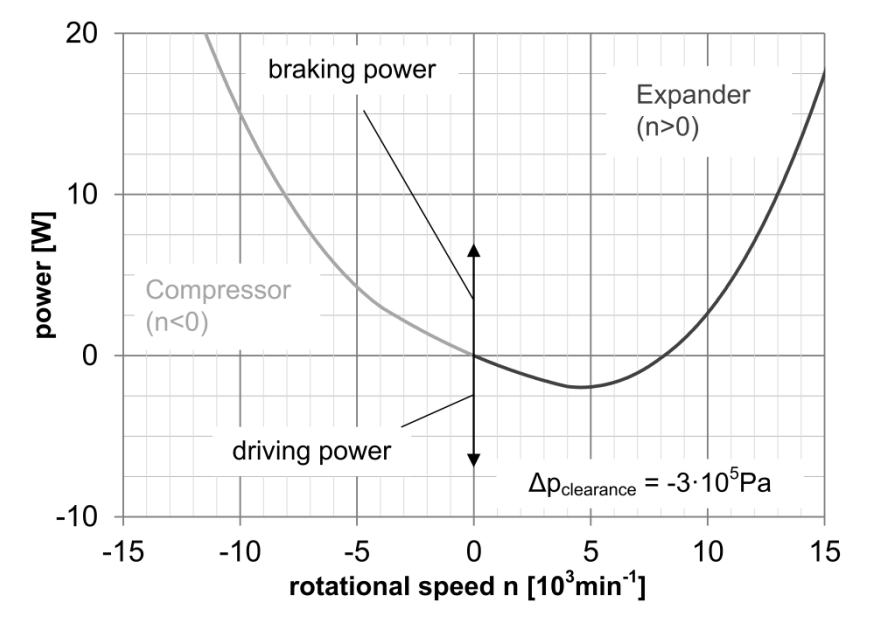

Fig. 11: Transferred frictional power as a function of rotational speed n for male rotor front clearance of the GL51 screw type machine

generated. If the screw machine is applied as compressor, Poiseuille flow resulting from negative pressure difference and Couette flow always cause braking power as the direction of both flows is opposed to the rotor´s direction of rotation. For rotational speeds of an expander, driving power results which at first increases then decreases after the global maximum. This is based on two different effects of rotational speed. On the one hand, increasing rotational speed leads to rising driving power as emitted power generated by the torque of Poiseuille flow depends linearly on rotational speed. On the other hand an increase in rotational speed leads to a quadratically rising braking power by Couette flow. For pure laminar flow, the power curve would be an ideal parabola. Nevertheless, the curve shown in figure 11 does not exactly correspond to a parabola due to occurring turbulences.

Modelling of flow through housing clearances

Geometric modelling of male rotor housing clearance is illustrated in **figure 12**. The contours of rotor and housing are described by a finite number of plane wall elements connected in series. It is assumed that clearance geometry is described by the shortest connection of bounding chambers. Therefore the section shown in figure 12 is parallel to direction of flow and does not equal the rotor´s front section. Unknown pressure distribution must be derived by additional boundary conditions for each element. Due to the conservation of mass, overall mass flow is the same within all elements. Furthermore, the conservation of momentum leads to static pressure difference between two elements according to changing cross-section areas. Assuming isotherm, frictionless ideal change of state this pressure difference is given by

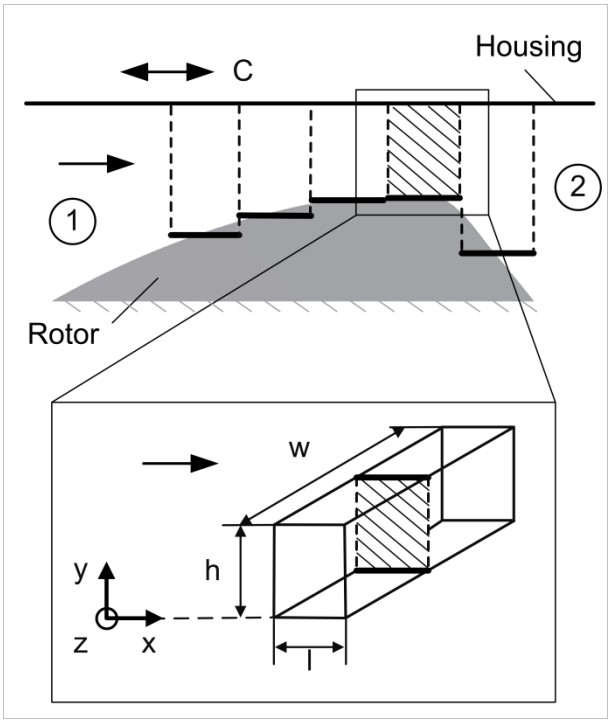

Fig. 12: Modelling housing clearance by finite number of wall elements

$$\Delta p_{i \rightarrow i+1} = \frac{\dot{m}^2}{2\rho w^2}\left(\frac{1}{h_i^2} - \frac{1}{h_{i+1}^2}\right)\Bigg|_{\text{frictionless}} . \qquad (7)$$

with clearance width w and element height h_i and h_{i+1} respectively. Taking frictional loss of pressure within elements into account, the overall pressure difference across the housing clearance is calculated by

$$\Delta p_{clearance} = \sum_{i=1}^{n} \Delta p_i \Big|_{frictional} + \sum_{i=1}^{n-1} \Delta p_{i \rightarrow i+1} \Big|_{frictionless} \tag{8}$$

where n is the number of flow elements. Thus the overall pressure difference consists of an irreversible, frictional part and a reversible ideal part that vanishes when $h_1 = h_n$. Note that equation (8) must be solved iteratively as mass flow cannot be expressed as an explicit function of pressure difference. For given mass flow, frictional pressure differences Δp_i are calculated according to equation (1) or equation (6) depending on either laminar or turbulent Poiseuille flow type of element i.

Furthermore flow direction illustrated in **figure 13** has to be considered. The geometry at the inlet of clearance corresponds to a nozzle. After the narrowest cross-section area, liquid flows through a diffuser geometry which has very large opening angles. Thus flow separation behind the narrowest cross-section area seems to be reasonable. Initial simulations have also shown very large positive pressure gradients in this region, which support the assumption of separation. Resulting simulated clearance geometry, dependent on flow direction, is shown in figure 13. Note that for several boundary conditions there might be no exact clearance flow solution as there is no solution for any geometry subsisting. Furthermore two solutions might exist, one for each geometry, which consequently leads to an undefined state of flow. Subsequently results for simulations at male rotor housing clearance of the GL 51 screw type machine are presented.

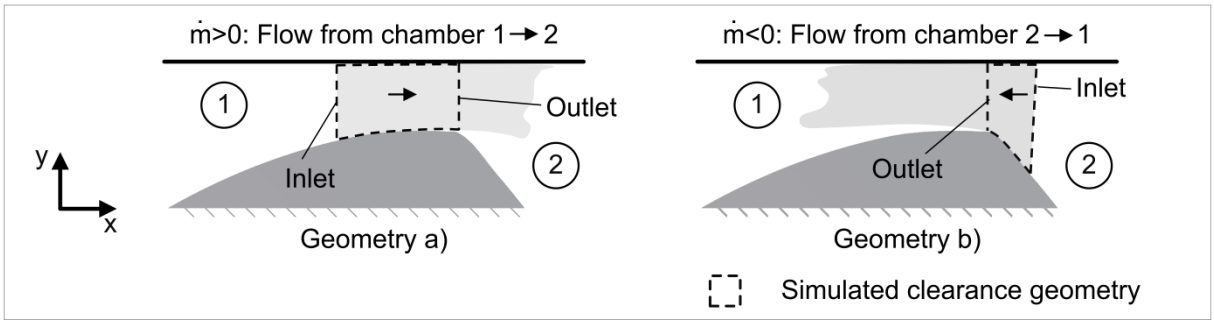

Fig. 13: Simulated clearance geometry of male rotor housing clearance depending on direction of flow

Simulation results for male rotor housing clearance

The previous described model is now applied to simulate male rotor housing clearance of the GL51 screw type machine using the auxiliary liquid water (ϑ = 25°C = const.). Minimum clearance height is set to 0.08 mm. Clearance height of 1 mm at the inlet of both geometries is estimated due to water volume that might exist in front of the clearance. Note that mass flow and transferred power depend proportionally on clearance width. Therefore all values are given per meter. Based on this mass flow transferred power seem to be huge compared to presented results of male rotor front clearance.

Figure 14 shows mass flow as a function of pressure difference. Furthermore, simulated geometry depending on direction of mass flow is given. For negative pressure differences the illustrated mass flow of compressor is larger than mass flow of expander. Analogues to front clearance flow, circumferential speed and negative pressure differences cause Couette and Poiseuille flow in the same direction within the housing clearance of compressor. In contrast, the expander´s opposed direction of rotation leads to reversed Couette flow (also see figure 1). In case of positive pressure differences, this relation turns around in both applications and the absolute value of expander mass flow is slightly bigger as Couette and Poiseuille flow show the same algebraic sign. It is apparent that influence of circumferential speed is distinctly smaller for geometry b). As previously mentioned, inlet clearance height of both geometries is set to 1 mm in order to have equal reversible impulse losses resulting from cross-section area reduction. Due to the rotor´s modified asymmetric SRM-Profile, the

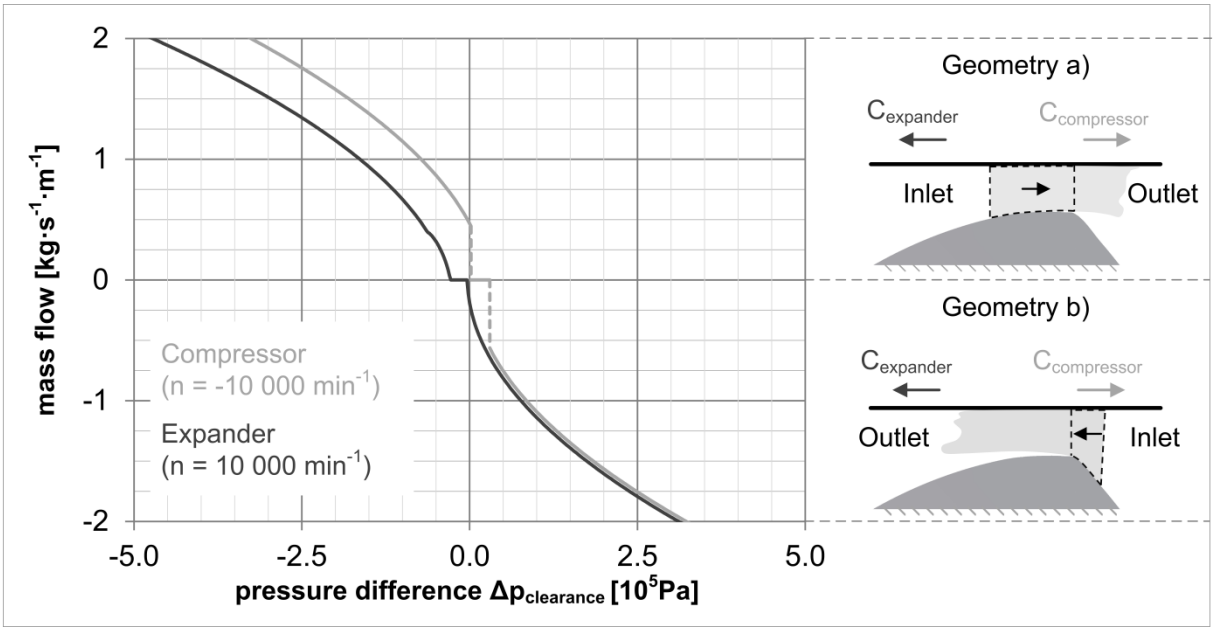

Fig. 14: Mass flow as a function of pressure difference $\Delta p_{clearance}$ for male rotor housing clearance of the GL51 screw type machine

equal inlet clearance heights of geometry a) and b) cause different clearance lengths resulting in different pressure gradients.

Influence of simulation geometry is demonstrated by geometrical variation illustrated in **figure 15**. Mass flow is shown as a function of pressure difference for simplified rotor geometries of geometry a). The goal of this simplification is to have a constant opening angle α along the rotor while the original geometry a), presented in figure 14, shows a variable opening angle. A relation between cross-section area difference of the in- and outlet and clearance length is described by α. Furthermore, mass flow dependent on pressure difference for non-viscous flow is given in figure 15. It is obvious that viscous flow converges at non-viscous flow for an increasing opening angle. To understand this, there are two limiting cases that have to be considered. For an angle of α = 90° geometry a) corresponds to an ideal orifice and no friction occurs. Therefore, circumferential speed causes only relative velocity of the orifice but no drag force leading to fluid acceleration. The smallest opening angle of geometry b) is α = 45°. Thus both mass flow functions shown in figure 14 almost correspond to non-viscous flow for geometry b). The other limiting case is α = 0 for which reversible pressure difference based on reduction of cross-section area disappears. Therefore, flow is equivalent to flow between previously described parallel moving walls which are only influenced by frictional effects. Consequently the influence of the rotor´s drag force rises. At the clearance inlet of geometry a) opening angle α is larger than the angles of the shown simplified geometries. Based on the small mass flow it seems that the overall flow

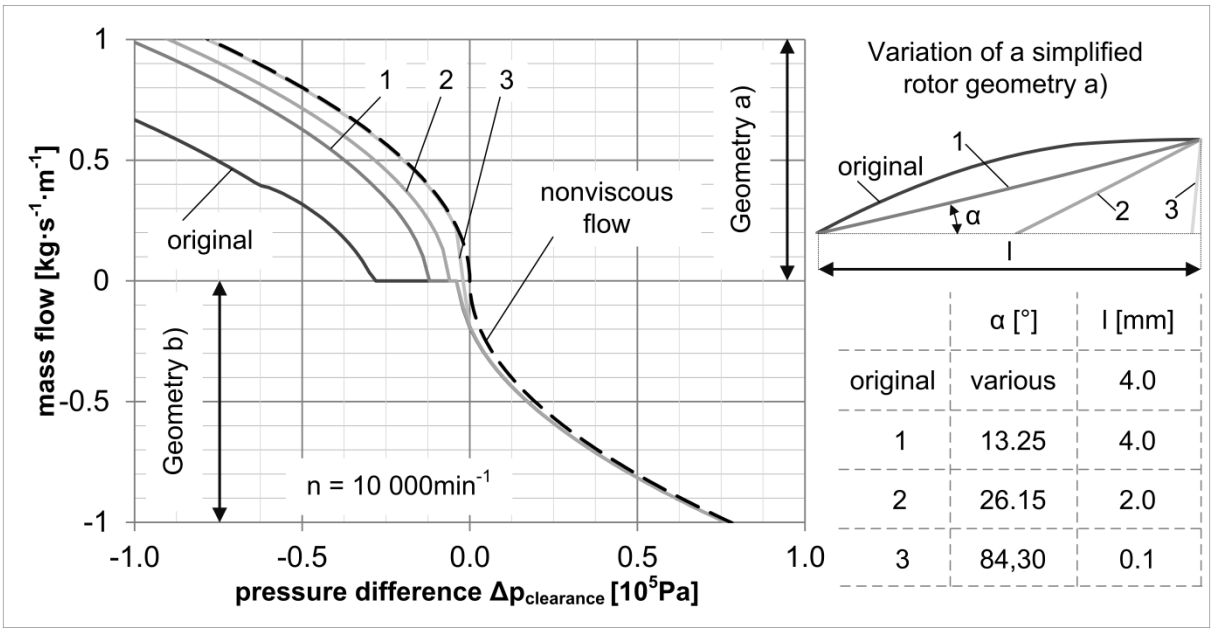

Fig. 15: Mass flow as a function of pressure difference $\Delta p_{clearance}$ for various simplifications of rotor geometry a)

of geometry a) is mainly influenced by the almost vanishing α at the clearance outlet. Thus mass flow is a lot more affected by circumferential speed for simulation geometry a).

As previously mentioned there are undefined states of flow at housing clearances. In this case, mass flow is set to zero as no reasonable solution can be calculated. Therefore, mass flow functions in figure 14 and 15 are unsteady. Note that this effect vanishes for symmetric geometries.

In addition to mass flow, transferred power resulting from friction at the rotor´s surface is also an interesting quantity. **Figure 16** demonstrates power as a function of pressure difference for both expander and compressor. Again, negative algebraic sign represents driving force whereas positive sign corresponds to power consumption of working fluid. Dashed lines mark undefined states of flow. For these operational parameters linear interpolation of transferred power seems to be reasonable. Nevertheless, these values cannot be calculated directly by using above mentioned theory.

In case of negative pressure differences, auxiliary liquid transfers additional power to the rotor of an expander. This is based on Poiseuille flow, which flows in the rotor´s direction of rotation. Compared to male rotor front clearance, even small negative pressure differences cause driving force on the rotor´s surface, as very small length of housing clearance leads to high pressure gradients. Consequently, Poiseuille flow overcompensates braking Couette flow. In order to fulfil the conservation of mass, pressure-driven Poiseuille flow, which results from internal pressure distribution, is present. This internal pressure distribution always exists

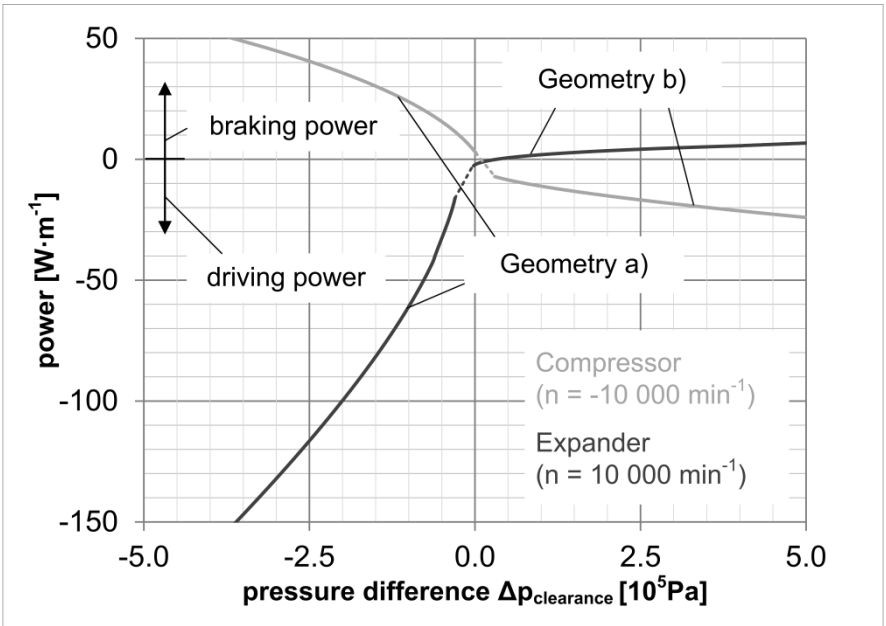

Fig. 16: Transferred frictional power as a function of pressure difference $\Delta p_{clearance}$ for male rotor housing clearance of the GL51 screw type machine

and changes with rotational speed. Thus Poiseuille flow depends on rotational speed as well as external pressure difference which is very different from independent effects within front clearances. Nevertheless, Couette flow is neither influenced by external nor internal pressure differences.

Relations between pressure difference and frictional power reverse for compressors due to opposed directions of rotation. Apparently the absolute value of transferred power is far greater for negative pressure differences. This is based on described different simulation geometries. As previously mentioned flow through geometry b) is very close to non-viscous flow which leads to an almost vanishing transferred frictional power. In comparison, viscous effects are much more important for flows through geometry a). Therefore different absolute values are not dominated by the algebraic sign of pressure difference, but instead by which simulation geometry is used.

Conclusion

Inherent different clearances cause internal leakage flows which significantly influence operational behaviour of screw machines. Therefore, considerable effort has been made to understand and predict compressible one-phase clearance flows. Due to greater interest in liquid-injected screw machines, a second fluid phase occurs in the machine. Thus an ultimate research goal is modelling a two-phase screw machine including clearance flows. Assuming that clearances are closed by auxiliary liquid, a first analytic model of incompressible, static, laminar and turbulent clearance flows through both front and housing clearances of screw machines is presented in this article. Complex clearance geometries are modelled by a finite number of parallel moving wall elements which are connected in parallel (front clearance) or in series (housing clearance). The latter requires additional boundary conditions at each element to determine axial pressure distribution along the direction of flow. Clearance mass flow and transferred frictional power are illustrated for both male rotor front and housing clearance of the GL51 screw type machine. It is remarkable that the rotor might be driven by friction within the clearance, provided that Poiseuille flow cancels out Couette flow. Required pressure differences are much smaller for male rotor housing clearances compared to male rotor front clearances. Furthermore, driving force occurs mainly within an expander.

Simulation geometry of male rotor housing clearance has remarkable influence on results. Therefore it is essential to put further effort into determining the distribution of liquid within screw machines in order to understand more about complex relations inside chambers and clearances. Subsequently, the theory presented should be applied to the working cycles of

screw machines to quantify overall clearance mass flow and resulting transferred power. Finally, comparing friction loss with improved sealing of clearances will be reasonable.

List of symbols

Symbol	Dimension	Meaning	Index	Meaning
A	m^2	area	an	analytic
c	$m \cdot s^{-1}$	velocity	cc	crown circle
C	$m \cdot s^{-1}$	wall velocity	crit	critical
d	m	diameter	C	Couette
h	m	clearance height	f	fluid
l	m	clearance length	i	element number
$\dot{m}$	$kg \cdot s^{-1}$	mass flow	m	mean
n	min^{-1}	rotational speed	$\dot{m}$	mass flow
p	$N \cdot m^{-2}$	pressure	n	number of elements
Δp	$N \cdot m^{-2}$	pressure difference	num	numeric
P	$N \cdot m \cdot s^{-1}$	power	P	Poiseuille
Re		Reynolds number	rc	root circle
w	m	clearance width	x,y,z	Cartesian
x,y,z	m	Cartesian coordinates		coordinates
α	rad	opening angle	τ	shear stress
η	$N \cdot s \cdot m^2$	dynamic viscosity		
κ		Von Kármán constant	G (K,D)	mathematical
ρ	kg·m-3	density		function to calculate
τ	$N \cdot m^{-2}$	shear stress		the inversion of the
ϑ	°C	temperature		law of resistance

References

[1] Janicki, M. (2007): Modellierung und Simulation von Rotationsverdrängermaschinen. Dissertation. University Dortmund

[2] Temming, J. (2007): Stationärer und instationärer Betrieb eines unsynchronisierten Schraubenladers. Dissertation. University Dortmund

[3] Fister, W.; Neumann, G. (1984): Berechnung der reibungsbehafteten Strömung in den Zahnlücken und Dichtspalten von Schraubenmaschinen. In: VDI-Tagung Schraubenmaschinen. VDI-Berichte 521. Düsseldorf: VDI Verlag, Pages 299-327

[4] Fleming, J.S.; Tang, Y. (1995): The Analysis of Leakage in a Twin Screw Compressor and its Application to Performance Improvement. In: Proceedings of the Institution of Mechanical Engineers, Part E: Journal of Process Mechanical Engineering 209 (2), Pages 125-136

[5] Sachs, R. (2002): Experimentelle Untersuchung von Gasströmungen in Schraubenmaschinen. Dissertation. University Dortmund

[6] Kauder, K.; Stratmann, D. (2002): Numersiche Strömungsuntersuchung der Gasspaltströmung am Hauptrotor-Gehäusespalt in Schraubenmaschinen. In: Schraubenmaschinen (10), Pages 49-62

[7] Kauder, K. (1979): Energiewandlung in öleingespritzen Schraubenverdichtern. In: Technische Mitteilungen 72 (6), Pages 404-410

[8] Harling, B. (1993): Untersuchung zur Ölverteilung in Schraubenkompressoren mit Schmiermitteleinspritzung. Dissertation. University Dortmund

[9] Wincek, M. (1992): Zur Berechnung des Förderverhaltens von Schraubenspindelpumpen bei der Förderung von Flüssigkeits/Gas-Gemischen. Dissertation. Friedrich-Alexander University Erlangen-Nürnberg

[10] Schlichting, H.; Gersten, K. (2006): Grenzschichttheorie. Springer-Verlag, Berlin [u.a.], 10th edition

[11] Gersten, K.; Herwig, H. (1992): Strömungsmechanik. Vieweg, Braunschweig [et al.]

Acknowledgement

Supported by:

Federal Ministry for Economic Affairs and Energy on the basis of a decision by the German Bundestag